ChemComm

Accepted Manuscript

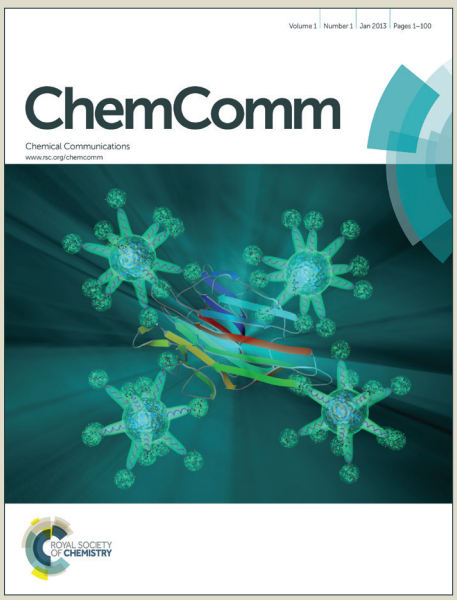

ROYAL SOCIETY OF CHEMISTRY

www.rsc.org/chemcomm

Journal Name

RSCPublishing

COMMUNICATION

Cite this: DOI: 10.1039/x0xx00000x

Three-Dimensional NiFe Layered Double Hydroxide Film for High-efficiency Oxygen Evolution Reaction

Received 00th January 2012,
Accepted 00th January 2012

DOI: 10.1039/x0xx00000x

www.rsc.org/

Zhiyi Lu[†a], Wenwen Xu[†a], Wei Zhu[a], Qiu Yang[a], Xiaodong Lei[a], Junfeng Liu[a], Yaping Li[a], Xiaoming Sun*[a] and Xue Duan[a]

Fabricating active materials into specific macrostructures is critical in the pursuit of high electro-catalytic activity. Herein we demonstrate that building a three-dimensional (3D) architecture of NiFe layered double hydroxide (NiFe-LDH) significantly reduced the onset potential, yielded high current density at small overpotentials, and showed an outstanding stability in electrochemical oxygen evolution reaction.

Layered double hydroxides (LDHs), also known as anionic or hydrotalcite-like clays, are composed of layers of divalent and trivalent metal cations coordinated to hydroxide anions, with guest anions (typically CO_3^{2-}) intercalated between the layers.[1, 2] LDHs have been widely studied in fields of catalysts[3, 4], flame retardants[5], drug delivery hosts[6], and as biomaterials[7]. Recently, their applications as electro-active materials in supercapacitors and fuel cells are attracting considerable attentions.[8, 9] Searching for new compounds composed of abundant and inexpensive elements[10, 11], as alternatives for traditional OER catalysts, should be the key to developing practical applications of a number of energy storage and conversion processes, including water splitting and metal–air batteries[12-15]. Latest report demonstrates NiFe-based LDH has shown a superb activity than either of the parent metal catalyst, and comparable to the best noble catalysts (e.g. IrO_2 and RuO_2) for oxygen evolution reaction (OER)[16]. However, issues of limited specific surface area and conductivity should be further addressed before practical application of LDHs as electrode materials.[17, 18]

Directly constructing 3D architecture on conductive metal substrates can partially overcome the above issues and thereby bring about a dramatic improvement in the electrochemical performance of the active material.[19-24] Compared to the conventional 2D planar architecture, electrodes based on 3D porous architecture can offer several critical advantages, such as facilitating electron transportation, promoting electrolyte penetration and increasing the electrochemically active surface area.[25, 26] Recent work has confirmed the great benefit of 3D architecture on enhancing the OER activity.[27, 28] Therefore, 3D NiFe-LDH film can be anticipated to show excellent electro-catalytic performance. Moreover, the easy accessibility of LDHs based 3D film[29] should facilitate their commercial production.

In this work, 3D films of vertically aligned NiFe-LDH nanoplates (NiFe-LDH NPs) loaded on nickel foam have been fabricated for use as electrodes for OER (Fig. 1A). The nickel foam was chosen here (Fig. 1B) because of its zig-zag skeleton and high porosity, which helped to increase the active surface area.[22, 27] *In situ* growth of NiFe-LDH NPs resulted in an oriented and rigid 3D architecture, which should help to overcome the problem of low conductivity in conventional LDH films. The electrochemical results demonstrated the NiFe-LDH film could afford a low onset potential (~1.46 V vs. RHE) and a fast current increase, thanks to the synergistic effect of the intrinsically high activity of the catalyst and the unique 3D architecture. Accordingly, only a small overpotential was required (~1.51 V) for achieving 30 $mA \cdot cm^{-2}$ (η_{30}), better than that of 3D $Ni(OH)_2$ film and 20 wt% Ir/C catalyst. In addition, this catalyst film showed prominent durability when continuously operating OER at high rates.

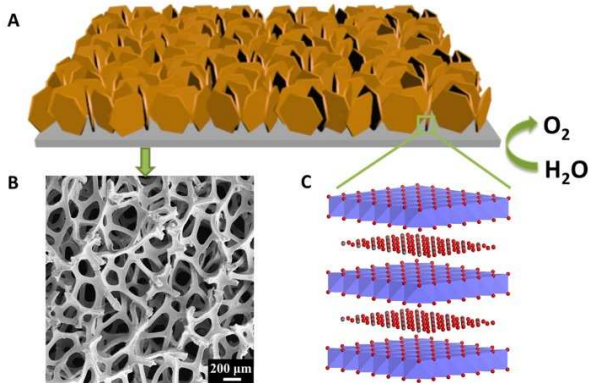

Figure 1. (A), Schematic illustration of NiFe-LDH nanoplates grown on nickel foam; (B), the SEM image of nickel foam; (C) the crystal structure of LDHs.

The 3D NiFe-LDH NP film was synthesized using nickel and iron nitrates as metal source and urea as the precipitant under hydrothermal condition at 120°C (see experimental section). At this temperature, urea decomposed into ammonia which created alkaline environment, and carbonate which served as the intercalated anion. After hydrothermal reaction, a brown film was coated on the surface of nickel foam (Fig. 2A), indicating the successful growth of NiFe-LDH. SEM images of the as-synthesized NiFe-LDH film at different magnifications (Figs. 2B and 2C) showed that the LDH film was mesoporous with nanoplates growing vertically on the Ni substrate. The distance between nanoplates was ~100 nm and the film thickness was approximately 200–300 nm (inset of Fig. 2B). An individual nanoplate from the film had a crumpled and hexagonal morphology, with a lateral size of ~200 nm and was very thin, as revealed by TEM (inset of Fig. 2C). The coincidence of the nanoplate size with film thickness suggested that the NiFe-LDH NPs were directly grown on the Ni substrate as intact units.

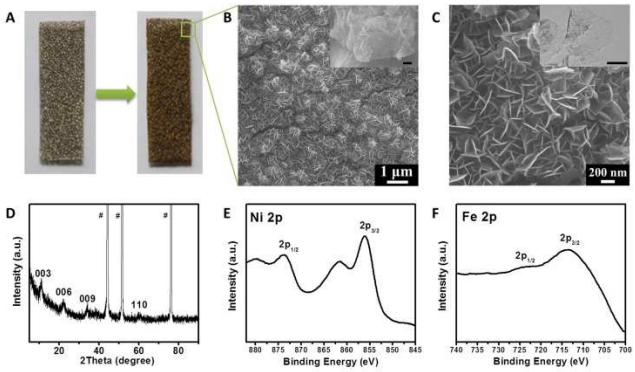

Figure 2. (A), optical images of nickel foam before (left) and after (right) growing NiFe-LDH NP film; (B) and (C), low- and high-magnification SEM images of NiFe-LDH NP film, inset: cross-view SEM image and typical TEM image, scale bar: 100 nm; (D), XRD pattern of NiFe-LDH NP film; (E) and (F), XPS spectra of Ni and Fe in NiFe-LDH NP film. These results demonstrate the NiFe-LDH NPs are uniformly and directly grown on nickel foam.

X-ray diffraction (XRD) and X-ray photoelectron spectroscopy (XPS) were employed to verify the phase and composition of NiFe-LDH NPs. XRD data showed a series of Bragg reflections, which matched well with the typical profile for LDH materials (the peaks marked "#" denoted the Ni substrate, Fig. 2D).[30] XPS results confirmed the presence of both Fe and Ni in the film surface (Fig. S1). The binding energy of Ni $2p_{3/2}$ and Fe $2p_{3/2}$ located on 855.7 eV and 713.7 eV (Fig. 2E and F), respectively, indicating the +2 and +3 oxidation states of Ni and Fe.[16] The atomic ratio of Ni and Fe was ~3:1, confirming the composition of NiFe-LDH along with the XRD data. EDX mapping analysis (Fig. S2) showed that both the nickel and iron elements were homogeneously distributed in the cross-linked 3D architecture.

Such a 3D porous film should promote electrochemical reactions on the electrode surface by exposing more active sites[27, 31]. Therefore we investigated the NiFe-LDH NP films as potential electro-catalytic electrodes for OER in O_2 saturated 0.1 M KOH solution using a typical three-electrode setup. The potential calibration of the reference electrode was shown in Fig. S3.[32] A β-$Ni(OH)_2$ NP film (details were shown in Fig. S4) and a pure nickel foam (Fig. S5) were also tested as control samples. Representative cyclic voltammograms (Fig. 3A) revealed that the β-$Ni(OH)_2$ NP film exhibited two primary characteristics: a redox couple at 1.35 V vs. the reversible hydrogen electrode (RHE), which was attributed to the transformation between $Ni(OH)_2$ and NiOOH[33]; and a positive (oxidation) current at potentials greater than 1.5 V, which was ascribed to OER. These two features were also visible on NiFe-LDH NP film, but there were noticeable differences. The $Ni(OH)_2$/NiOOH redox couple in the LDH film occurred at a higher potential, suggesting the conversion from Ni(II) to Ni(III) was inhibited by the highly charged Fe(III) ions occupying the surrounding positions, consistent with previous reports[34, 35]. However, the OER of LDH started at a less positive potential than that of $Ni(OH)_2$, indicating the NiFe-LDH phase was more desirable for OER. Polarization curve (Fig. 3B) recorded with our NiFe-LDH NP film showed an early onset of ~1.46 V (correlate to overpotential of ~230 mV, which was determined by the start point of Tafel slope), beyond which the anodic current rose rapidly under more positive potentials. Consequently, a high OER rate (e.g. 30 mA·cm^{-2}) could be achieved only requiring a small overpotential (an η_{30} of ~280 mV), much better than that of β-$Ni(OH)_2$ NP film (~450 mV) and pure nickel foam (~520 mV). It should be noted that the OER activity of NiFe-LDH NP film was even better than 20 wt% Ir/C catalyst (XRD pattern can be seen in Fig. S6), which afforded an onset potential of 1.5 V and a η_{30} of ~390 mV, highlighting the advanced 3D structural design.

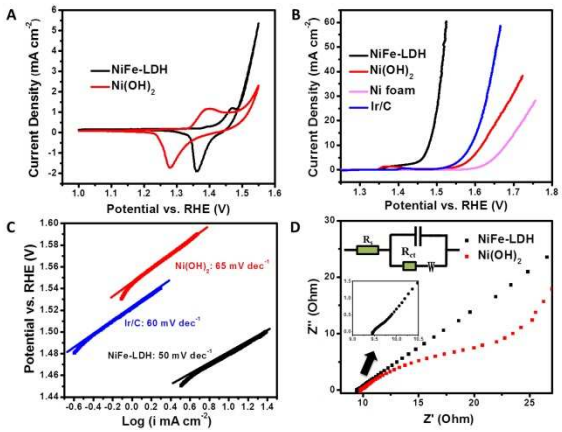

Figure 3. (A), CV curves of NiFe-LDH and $Ni(OH)_2$ NP films; (B), Polarization curves of various catalysts; (C), Tafel plots on NiFe-LDH NP film (black), $Ni(OH)_2$ NP film (red) and 20 wt% Ir/C catalyst (blue). (D), Nyquist plots of NiFe-LDH and $Ni(OH)_2$ NP films, and the corresponding equivalent circuit. Based on these results, we can conclude that the NiFe-LDH NP film shows the optimal activity for OER.

To gain more insight into the OER activity, Tafel plots derived from polarization curves were constructed (Fig. 3C). The resulting Tafel slope of NiFe-LDH NP film was ~50 mV·dec^{-1}, which was smaller than that of β-$Ni(OH)_2$ NP film (~65 mV·dec^{-1}) and Ir/C catalyst (~60 mV·dec^{-1}), indicating the NiFe-LDH NP film exhibited the highest OER activity. The Tafel slope observed for the NiFe-LDH NP film was close to the value (40 mV·dec^{-1}) characteristic of a mechanism involving a pre-equilibrium consisting of a one-electron electrochemical step with a possible chemical step, followed by a one-electron electrochemical rate determining step.[36] Electrochemical impedance results (Fig. 3D) demonstrated that NiFe-LDH possessed a much smaller charge transfer resistance (R_{ct} in the equivalent circuit) than that of β-$Ni(OH)_2$, indicative of a much faster electron transfer process during electrochemical reaction.[37] This may because the broader interlayer spacing of the NiFe-LDH favors the ion diffusion to the active materials.

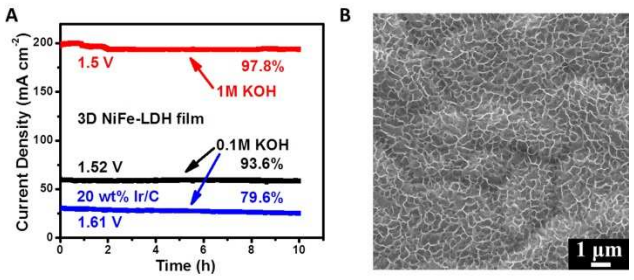

Figure 4. (A), Stability testing of NiFe-LDH NP film under constant potentials in 0.1 M and 1 M KOH solution and 20 wt% Ir/C catalyst; (B), SEM image of NiFe-LDH after stability testing. These results indicate that NiFe-LDH NP film shows an outstanding stability for OER.

The long-term durability of a catalytic electrode is another crucial issue to consider for practical applications, especially for these porous and nanostructured films. When operating the OER at constant overpotentials, stable corresponding current densities were observed on 3D LDH electrodes, in both 0.1 M (~60 mA·cm^{-2}) and 1 M KOH solutions (~200 mA·cm^{-2}) with negligible degradations (6.4% and 2.2%, respectively) after 10h testing (Fig. 4A), revealing its excellent stability under OER condition. This was ascribed to the tight binding between the active material and the substrate, which was evidenced by the ultrasonication testing (Fig. S7). Moreover, the surface structure of NiFe-LDH NP film was essentially retained after OER for 10 hours (Fig. 4B), further demonstrating the robustness of the electrode. This benefit afforded by the 3D architecture was confirmed by the high stability of $Ni(OH)_2$ NP film (Fig. S8) while, in contrast, the current density of the drop-cast Ir/C film decreased gradually with time (maintaining less than 80% of the initial current density after 10 h, as shown by the blue line in Fig. 4A). Combining the above merits, this 3D NiFe-LDH NP electrode was among the most active non-precious 3D metal electrocatalysts (see comparison in Table S1).[28, 38]

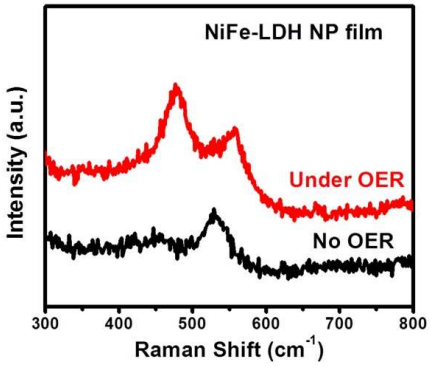

Figure 5. *In-situ* Raman spectroscopy of NiFe-LDH films with (1.6 V vs. RHE) and without OER operating.

Understanding the source of the ultrahigh OER activity is critical for designing even better electrodes. Here we employed an in situ Raman technique to probe the possible reason for the excellent OER activity. Two potentials (1.2 V and 1.6 V vs. RHE) were applied to the films to create different conditions (i.e. without and with OER, respectively). At 1.2 V, where OER did not occur, the Raman spectrum of the NiFe-LDH film showed a broad band located at 528 cm^{-1} (Fig. 5), in good accordance with the observation of NiFe oxide film, suggesting that the NiFe-LDH was disordered.[39] Under an oxygen evolution potential of 1.6 V, the disappearance of the former band and the appearance of two new bands (at 476 and 556 cm^{-1}) indicated the conversion from the LDH into NiOOH[40], similar to what was observed for $Ni(OH)_2$ (Fig. S9), demonstrating NiOOH was the active phase for OER. However, the weaker intensities and broader nature of the pair of NiOOH bands in NiFe-LDH compared with those in the case of $Ni(OH)_2$ reflected the more complex local environments around Ni–O, and suggested that the NiFe-LDH film possessed more structural defects. Ni is regarded as the active site for OER, but we believe that Fe incorporation into Ni hydroxides could create more active sites and thereby enhance the OER activity.

This 3D porous architecture of LDH offers several advantages when used for OER. The first advantage of our material was the directly grown catalyst layer that eliminated the need for polymer binders (which imparted additional resistance) and thereby provided an efficient pathway for electron transport through the entire electrode. Secondly, owing to the aggregation-free architecture of the vertically aligned nanoplates, the 3D electrode had a much larger surface area (by a factor of ~4, according to Brunauer–Emmett–Teller measurements, Table S2) than that of the bare current collector, suggesting a high density of active sites for OER. Thirdly, the nanostructured electrode consisted of nanosized units which formed a system of nanopores, thus facilitating electrolyte diffusion. Accordingly, this electrode gave a high current density (~60 mA·cm^{-2}). Moreover, the OER activity of the NiFe-LDH NP electrode in 1 M KOH solution was much higher with a lower Tafel slope (~43 mV·dec^{-1}) and a higher current density (~200 mA·cm^{-2}) at a potential of 1.5 V (Fig. S10).

In summary, a novel 3D porous film consisting of vertically aligned NiFe-LDH NPs was developed to realize high efficient water oxidation. The NiFe-LDH NP film exhibited excellent OER performance with small onset overpotential (~230 mV), low Tafel slope (~50 mV·dec^{-1}), large anodic current density (a η_{30} of 280 mV) and prominent electrochemical durability. They are mainly attributed to combination of the highly active NiFe-LDH phase with unique hierarchical mesoporous 3D architectures. This study affords a new strategy to achieve optimal performance in 3D catalysts, which may be extended to the preparation of other 3D hybrid materials for a broad range of technological applications.

Notes and references

[a] *State Key Laboratory of Chemical Resource Engineering, Beijing University of Chemical Technology, Beijing 100029, China*
Tel.: +86-10-64448751. Fax: +86-10-64425385.
E-mail: sunxm@mail.buct.edu.cn
† Contributed equally to this work

Electronic Supplementary Information (ESI) available: [experimental section, XPS survey, mapping data, SEM and XRD results, electrochemical testing, *in-situ* raman data and specific surface area results]. See DOI: 10.1039/c000000x/

1. Q. Wang and D. O'Hare, *Chem. Rev.*, 2012, **112**, 4124-4155.
2. D. G. Evans and R. C. Slade, in *Layered double hydroxides*, Springer, Berlin, 2006, pp. 1-87.
3. B. Sels, D. De Vos, M. Buntinx, F. Pierard, A. Kirsch-De Mesmaeker and P. Jacobs, *Nature*, 1999, **400**, 855-857.

4. X. Xu, R. Lu, X. Zhao, S. Xu, X. Lei, F. Zhang and D. G. Evans, *Appl. Catal. B: Environ.*, 2011, **102**, 147-156.
5. C. Manzi-Nshuti, J. M. Hossenlopp and C. A. Wilkie, *Polym. Degrad. Stab.*, 2009, **94**, 782-788.
6. A. Alcantara, P. Aranda, M. Darder and E. Ruiz-Hitzky, *J. Mater. Chem.*, 2010, **20**, 9495-9504.
7. H. B. Yao, Z. H. Tan, H. Y. Fang and S. H. Yu, *Angew. Chem. Int. Ed.*, 2010, **49**, 10127-10131.
8. Z. Lu, W. Zhu, X. Lei, G. R. Williams, D. O'Hare, Z. Chang, X. Sun and X. Duan, *Nanoscale*, 2012, **4**, 3640-3643.
9. Y. Wang, H. Ji, W. Peng, L. Liu, F. Gao and M. Li, *Int. J. Hydrogen. Energ.*, 2012, **37**, 9324-9329.
10. D. Wang and Y. Li, *Adv. Mater.*, 2011, **23**, 1044-1060.
11. D. Wang, Q. Peng and Y. Li, *Nano Res.*, 2010, **3**, 574-580.
12. M. W. Kanan and D. G. Nocera, *Science*, 2008, **321**, 1072-1075.
13. J. Suntivich, K. J. May, H. A. Gasteiger, J. B. Goodenough and Y. Shao-Horn, *Science*, 2011, **334**, 1383-1385.
14. R. D. Smith, M. S. Prévot, R. D. Fagan, Z. Zhang, P. A. Sedach, M. K. J. Siu, S. Trudel and C. P. Berlinguette, *Science*, 2013, **340**, 60-63.
15. J.-J. Xu, Z.-L. Wang, D. Xu, L.-L. Zhang and X.-B. Zhang, *Nat. Commun.*, 2013, **4**, 2438-2447.
16. M. Gong, Y. Li, H. Wang, Y. Liang, J. Z. Wu, J. Zhou, J. Wang, T. Regier, F. Wei and H. Dai, *J. Am. Chem. Soc.*, 2013, **135**, 8452-8455.
17. L. Wang, D. Wang, X. Dong, Z. Zhang, X. Pei, X. Chen, B. Chen and J. Jin, *Chem. Commun.*, 2011, **47**, 3556-3558.
18. Y. Wang, W. Yang, C. Chen and D. G. Evans, *J. Power Sources*, 2008, **184**, 682-690.
19. C. K. Chan, H. Peng, G. Liu, K. McIlwrath, X. F. Zhang, R. A. Huggins and Y. Cui, *Nat. Nanotech.*, 2007, **3**, 31-35.
20. P. Simon and Y. Gogotsi, *Nat. Mater.*, 2008, **7**, 845-854.
21. J. Jiang, Y. Li, J. Liu, X. Huang, C. Yuan and X. W. D. Lou, *Adv. Mater.*, 2012, **24**, 5166-5180.
22. Y. H. Chang, C. T. Lin, T. Y. Chen, C. L. Hsu, Y. H. Lee, W. J. Zhang, K. H. Wei and L. J. Li, *Adv. Mater.*, 2013, **25**, 756-760.
23. H. Wang, D. Kong, P. Johanes, J. J. Cha, G. Zheng, K. Yan, N. Liu and Y. Cui, *Nano Lett.*, 2013, **13**, 3426-3433.
24. J. Kibsgaard, Z. Chen, B. N. Reinecke and T. F. Jaramillo, *Nat. Mater.*, 2012, **11**, 963-969.
25. X. Lang, A. Hirata, T. Fujita and M. Chen, *Nat. Nanotech.*, 2011, **6**, 232-236.
26. Z. Lu, Q. Yang, W. Zhu, Z. Chang, J. Liu, X. Sun, D. G. Evans and X. Duan, *Nano Res.*, 2012, **5**, 369-378.
27. J. Wang, H. x. Zhong, Y. l. Qin and X. b. Zhang, *Angew. Chem. Int. Ed.*, 2013, **125**, 5356-5361.
28. J. Moir, N. Soheilnia, P. O'Brien, A. Jelle, C. M. Grozea, D. Faulkner, M. G. Helander and G. A. Ozin, *ACS nano*, 2013, **7**, 4261-4274.
29. X. Guo, F. Zhang, D. G. Evans and X. Duan, *Chem. Commun.*, 2010, **46**, 5197-5210.
30. G. Abellán, E. Coronado, C. Martí-Gastaldo, E. Pinilla-Cienfuegos and A. Ribera, *J. Mater. Chem.*, 2010, **20**, 7451-7455.
31. Y. Li, P. Hasin and Y. Wu, *Adv. Mater.*, 2010, **22**, 1926-1929.
32. P. D. Tran, M. Nguyen, S. S. Pramana, A. Bhattacharjee, S. Y. Chiam, J. Fize, M. J. Field, V. Artero, L. H. Wong and J. Loo, *Energy Environ. Sci.*, 2012, **5**, 8912-8916.
33. H. Wang, H. S. Casalongue, Y. Liang and H. Dai, *J. Am. Chem. Soc.*, 2010, **132**, 7472-7477.
34. C.-C. Hu and Y.-R. Wu, *Mater. Chem. Phys.*, 2003, **82**, 588-596.
35. R. Singh, J. Pandey and K. Anitha, *Int. J. Hydrogen Energy*, 1993, **18**, 467-473.
36. E. Castro and C. Gervasi, *Int. J. Hydrogen. Energ.*, 2000, **25**, 1163-1170.
37. T. Wang, L. Liu, Z. Zhu, P. Papakonstantinou, J. Hu, H. Liu and M. Li, *Energy Environ. Sci.*, 2013, **6**, 625-633.
38. W. Zhou, X. Xu, X. Cao, X. Huang, C. Tan, J. Tian, H. Liu, J. Wang and H. Zhang, *Energy Environ. Sci.*, 2013, **6**, 2216-2221.
39. M. W. Louie and A. T. Bell, *J. Am. Chem. Soc.*, 2013, **135**, 12329-12337.
40. J. Desilvestro, D. A. Corrigan and M. J. Weaver, *J. Electrochem. Soc.*, 1988, **135**, 885-892.

